JOURNAL OF THE ROYAL SOCIETY Interface

J. R. Soc. Interface (2005) **2**, 63–69
doi:10.1098/rsif.2004.0022
Published online 8 February 2005

Characterization of the elastic properties of the nuclear envelope

A. C. Rowat[1], L. J. Foster[2], M. M. Nielsen[2], M. Weiss[1] and J. H. Ipsen[1,†]

[1]*MEMPHYS—Center for Biomembrane Physics, Department of Physics, and* [2]*CEBI, Department of Biochemistry & Molecular Biology, Campusvej 55, University of Southern Denmark, 5230 Odense M, Denmark*

Underlying the nuclear envelope (NE) of most eukaryotic cells is the nuclear lamina, a meshwork consisting largely of coiled-coil nuclear intermediate filament proteins that play a critical role in nuclear organization and gene expression, and are vital for the structural stability of the NE/nucleus. By confocal microscopy and micromanipulation of the NE in living cells and isolated nuclei, we show that the NE undergoes deformations without large-scale rupture and maintains structural stability when exposed to mechanical stress. In conjunction with image analysis, we have developed theory for a two-dimensional elastic material to quantify NE elastic behaviour. We show that the NE is elastic and exhibits characteristics of a continuous two-dimensional solid, including connections between lamins and the embedded nuclear pore complexes. Correlating models of NE lateral organization to the experimental findings indicates a heterogeneous lateral distribution of NE components on a mesoscopic scale.

Keywords: mechanics; confocal laser scanning microscopy; micropipette aspiration; green fluorescent protein-lamin A; nucleoporin p62

1. INTRODUCTION

Compartmentalizing the cell's genetic material, the nuclear envelope (NE) forms a boundary between the nucleoplasm and cytoplasm of eukaryotic cells and embeds nuclear pore complexes (NPCs) that help to regulate nuclear composition. From a mechanical perspective, the NE is a complex, composite structure consisting of NPCs spanning both inner and outer membranes (INM and ONM) that are separated by the nuclear lumen. Associated with the INM is the nuclear lamina, a filamentous structure consisting primarily of lamin type B (expressed in all cell types) and type A/C proteins (expressed only in differentiated cells) that interact with integral membrane proteins, chromatin (Mattout-Drubezki & Gruenbaum 2003; Zastrow *et al.* 2004), chromatin-binding proteins (Zastrow *et al.* 2004) and nuclear actin (Bettinger *et al.* 2004; Shumaker *et al.* 2003). The lamina's insolubility under harsh extraction conditions (Aebi *et al.* 1986; Moir *et al.* 2000; Aaronsen & Blobel 1975) and fragile nuclear phenotypes characteristic of laminopathic diseases (Lammerding *et al.* 2004; Mounkes *et al.* 2003; Goldman *et al.* 2002) suggest that the lamina provides the nucleus with structural integrity. Models of the lamina as a regular lattice network supporting the NE (Alberts *et al.* 2002; Lodish *et al.* 2001; Boal 2002) are based largely upon evidence of patches of regular lattice structure of the lamina in amphibian *Xenopus oocyte* NEs (Aebi *et al.* 1986), but to what extent this model reflects lamina structure in other cell types is unresolved. Indeed, evidence of a thick, non-homogeneous lamina structure in vertebrate cells (Fawcett 1966; Paddy *et al.* 1990), as well as clusters of an integral INM lamin receptor protein (LBR) (Makatsori 2004), suggests an *irregular*, laterally heterogeneous NE structure. Despite the obvious contribution of the NE to nuclear shape and structure, a physical understanding of how this material provides the nucleus with structural stability has not been described. A quantitative characterization of the NE's physical properties is necessary for an understanding of the mechanisms underlying mitosis, NE-related diseases and viral infection, as well as how the nucleus is protected and affected by external forces (i.e. mechanotransduction).

To achieve this, we have analysed NE deformations in living *HeLa* cells transiently expressing green fluorescent protein fused to lamin A (GFP-LamA) using an extension of fluorescence imaged microdeformation (FIMD) (Discher *et al.* 1994) to confocal imaged microdeformation (CIMD). Nuclei are also isolated from these cells to investigate *in vitro* behaviour of both GFP-LamA and the NPCs that are visualized by staining with an antibody directed against the nucleoporin p62. We have developed image-analysis techniques in conjunction with theory for a two-dimensional elastic material to quantify NE elastic behaviour and demonstrate the similar behaviour of the NE both *in vivo* and *in vitro*. Together with modelling of the mesoscopic structure of the lamina, we

†Author for correspondence (ipsen@memphys.sdu.dk).

Received 29 September 2004
Accepted 23 November 2004

show that the NE is a material with a heterogeneous lateral organization that resists lateral shear forces and large-scale ruptures.

2. MATERIALS AND METHODS

2.1. Materials

All materials used were of the highest available quality and were obtained from the following sources: salts—Sigma (St Louis, USA); SYTOX Orange—Molecular Probes (Eugene, USA); Cy3-conjugated goat anti-mouse IgG—Jackson ImmunoResearch Laboratories, Inc. (West Grove, USA); p62 antinucleoporin IgG—BD Biosciences Pharmingen (San Diego, USA). Enhanced GFP fused to the amino terminus of the entire coding sequence for human prelamin A (GFP-LamA) was a kind gift from D. K. Shumaker and R. D. Goldman, Northwestern University, Chicago, USA (Moir *et al.* 2000).

2.2. Transfection

GFP-LamA amplified in Top10 cells and isolated using a Nucleobond AX plasmid purification protocol (Macherey-nagel, Duren) was transfected into subconfluent *HeLa* cells together with twofold excess carrier DNA (Herring testes DNA, Clontech, San Jose, USA) using $CaPO_4$ (Invitrogen, Carlsbad, USA).

2.3. Nuclear isolation

Nuclei were isolated from *HeLa* cells as previously described (Muramatsu *et al.* 1963). After centrifugation of the dounced nuclei, the supernatant was adjusted to have a final 'physiological' concentration (Jackson *et al.* 1988) of 130 mM KCl, 1.5 mM $MgCl_2$, 10 mM Na_2HPO_4, 1 mM Na_2ATP and 1 mM DTT, pH 7.4, in which the nuclear pellet was resuspended. All steps subsequent to trypsinization were carried out at 4 °C.

2.4. Confocal imaged microdeformation

Pipettes were pulled from glass capillary tubes (World Precision Instruments, Sarasota, USA) using a pipette puller (Sutter Instruments Co., USA) and forged (Microforge MF-900, Narishige, Japan) to ensure a flat pipette tip. The final inner diameter of the pipette was typically $2R_p = 2.5$–5.0 µm. Micropipettes were treated with silanization fluid (Number II, Sigma) and dried in an oven at 90 °C for about 2 h prior to aspiration to prevent adhesion of nuclei/cells to the glass surface. The micropipette was mounted on a Zeiss Axiovert 200M microscope equipped with a LSM 510 laser scanning module. Pressures were applied to nuclei through the micropipette using a custom built manometer system (Evans & Needham 1987). After applying pressure to interphase nuclei (identified as non-dividing, single, morphologically intact nuclei), the tongue length, L, stabilizes before acquiring an image. The pressure was incrementally increased in this manner, and nuclei were visualized. eGFP was excited using an argon laser (488 nm), and Cy3 using a He–Ne laser (543 nm). Multichannel acquisition was used to acquire images with more than one fluorophore. The pinhole size was typically set to approximately 1 Airy unit, resulting in a confocal slice thickness (z-resolution) of approximately 1 µm. *In vitro* nuclei were visualized in a two-well #1.0 borosilicate chamber (Nalge Nunc Int.) at room temperature (approximately 25 °C). For *in vivo* experiments, cells were grown on coverslips that were transferred to the viewing chamber at the time of the experiment and immersed in a CO_2-independent medium (minimum essential medium without phenol red containing 10% foetal bovine serum, 1% glutamate, 1% sodium pyruvate, 1% penicillin/streptomycin and 1% 1 M HEPES (Invitrogen)) at 37 °C. Three-dimensional reconstructions were generated using LSM 510 v. 3.0 software.

2.5. Modelling of intensity profiles

We take the thin elastic shell as a model for the NE and assume that the in-plane strain and stress can be described by a two-dimensional elastic model. Opposite to the situation in a fluid, the nearest neighbour structure of the NE is fixed, i.e. the molecular constituents are fixed relative to each other (characteristic of a solid), so for the purpose of modelling the surface is divided into elements, each of which contain some fixed surface components. In the equilibrium (undeformed) state, the characteristic length of an element is l_0. For a surface of revolution, such as the aspirated tongue of the NE in a micropipette, the elements along the meridian and latitude are labelled with the dimensions l_m and l_ϕ. We can write an approximate free energy density per element as (Ogden 1984; Stokke *et al.* 1986)

$$f = \frac{K}{2}\left(\frac{l_m l_\phi - l_0^2}{l_0^2}\right)^2 + \frac{\mu}{2}\left(\frac{l_m - l_\phi}{l_0}\right)^2. \qquad (2.1)$$

Here K and μ are the compression and shear moduli with units of J m^{-2}. Analysis of equation (2.1) shows that under micropipette deformation the density distribution in the cylindrical part of the shell is expected to decline exponentially throughout the pipette (along the x-axis) with the form $\rho(x) \propto \exp(-ax/R_p)$. This form holds if the NE behaves as a Hookean elastic sheet with $0 < a \leq 2$, where $a = 2$ for a simple homogeneous elastomer (Markin & Kozlov 1988). Fitting this expression to the experimental intensity profile data yields a value of a, a parameter that depends only on K/μ and the densities in the tongue tip and the bulk nucleus.

2.6. Modelling of intensity distributions

The observed pixel intensity distributions reflect the density and distribution of lamin proteins on a mesoscopic scale. Analysis and comparison of the mean intensity and variance to the predicted model behaviour provide insights into the underlying lamina structure. Details can be found in the Electronic Appendix.

3. RESULTS AND DISCUSSION

3.1. In vivo *nuclei*

In the initial state, the fluorescence intensity of GFP-LamA nuclei is localized primarily at the peripheral rim of the nuclei (inner nuclear membrane; figure 1*b*,*d*,*e*). Owing to the transient nature of the transfection, varying levels of GFP-LamA expression were observed, so only nuclei expressing medium levels of the construct (an intense rim and faint nucleoplasmic staining) were chosen for aspiration. A micropipette (inner radius $R_p \sim 1.5$–2.0 μm) was used to aspirate the nucleus through the plasma membrane of a living cell, and deformations of the nucleus were monitored by acquiring a series of confocal fluorescence images through the axial dimension in order to reconstruct a three-dimensional image. Under these conditions, the nuclear membrane and GFP-LamA-delineated lamina were both aspirated into the pipette (figure 1*i*). The fluorescence intensity is not homogenous throughout the extension in the pipette (tongue), but rather a gradient in fluorescence intensity is observed (figure 1*j*). As the fluorescence intensity (I) reflects the density of GFP-LamA (ρ), the observed tongue gradient signals the dilation of the lamins in the tip of the tongue, while the increased intensity about the mouth of the pipette indicates a local increase in the density (compression) of GFP-LamA. Although faint at the tongue tip, the GFP-LamA intensity is seen to coincide with the INM (figure 1*i*), indicating that the lamina remains associated with the NE despite the perturbation. The pixel intensity varies in the cylindrical tongue up to the edge of the hemispherical cap. The exponential form $\rho(x) \propto \exp(-ax/R_p)$ can be fit to this pixel intensity profile, where x is the position along the tongue (figure 1*j*,*k*). Our results for *in vivo* nuclei yield a small variation in a-values, $a = 0.41 \pm 0.04$ ($n = 7$)[1]. Together with the observed intensity ratio, $\langle I_i \rangle / \langle I_o \rangle = 0.5 \pm 0.1$, between the intensities in the aspirated tip (I_i) and bulk nucleus (I_o), this corresponds to an elastic moduli ratio, $K/\mu = 1.5 \pm 0.3$, where K is the expansion modulus and μ the shear modulus for a two-dimensional isotropic elastic material. From this deformational analysis, we conclude that the NE is a two-dimensional elastic material that resists shear forces like a solid.

The persistence of the intensity gradient over time (30–45 min) indicates that the structure of the underlying aspirated NE with which GFP-LamA is associated, remains constant. This observation is consistent with fluorescence recovery after photobleaching analyses that revealed slow recovery of GFP-lamin fusions in interphase cells (Daigle *et al.* 2001; Moir *et al.* 2000).

3.2. In vitro *nuclei*

Interpreting the aspiration of nuclei in whole cells is complicated by the presence of the cytoskeleton as well as various membranes and organelles. For this reason, isolated nuclei provide a much cleaner system in which other structural components, such as NPCs, can be indirectly labelled in order to further investigate

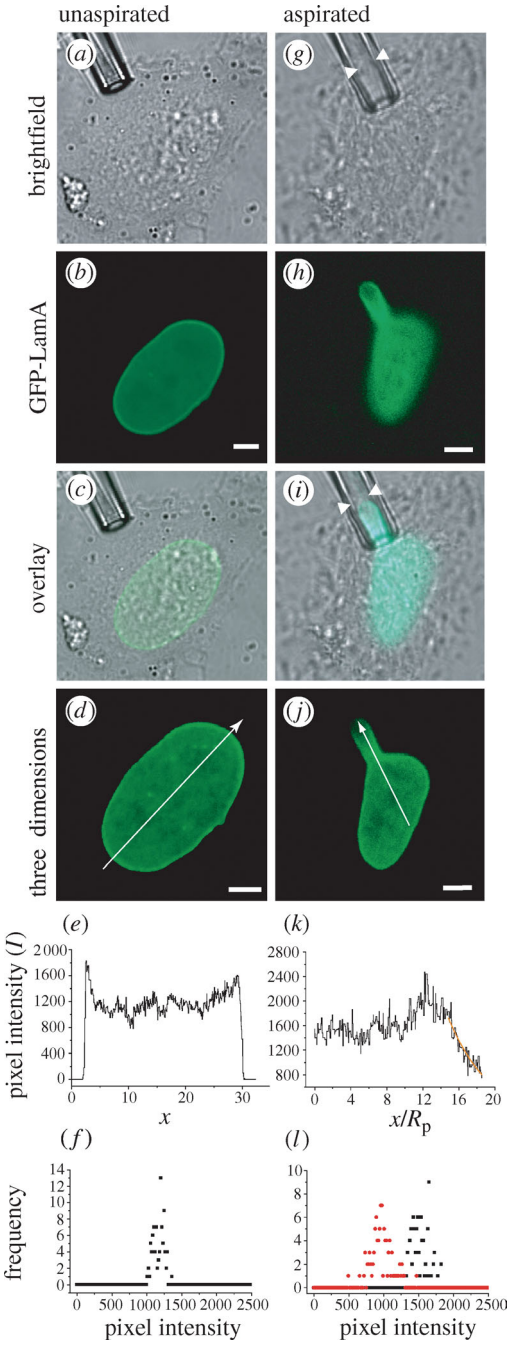

Figure 1. Non-homogeneous distribution of GFP-LamA upon deformation of nuclei *in vivo*. The nucleus of a *HeLa* cell transiently expressing GFP-LamA (*a*–*d*) is deformed by micropipette aspiration *in vivo* (*g*–*j*). Arrowheads show that the edge of the NE slightly precedes the GFP-LamA signal in the micropipette (*g*,*i*). The arrows through the three-dimensional reconstructions (*d*,*j*) illustrate how the intensity profiles (*e*,*k*) were generated. The maximum intensity corresponds to the mouth of the pipette. The exponential form $\rho(x) \propto \exp(-ax/R_p)$ is fit to the data (orange) and yields $a = 0.41 \pm 0.04$ ($n = 7$, $R_p = 1.6$ μm). Histograms of the pixel intensity were generated by sampling a 1.25 μm^2 area in unaspirated nuclei (*f*) and in the tongue tip (*l*, red) and bulk (*l*, black) of aspirated nuclei and show a heterogeneous density distribution of GFP-LamA. Scale bars represent 5 μm.

[1]In the region where the tongue extends out of the mouth, another form of apparent exponential behaviour was observed in some *in vivo* nuclei with $a^* = 0.09 \pm 0.01$ ($n = 5$).

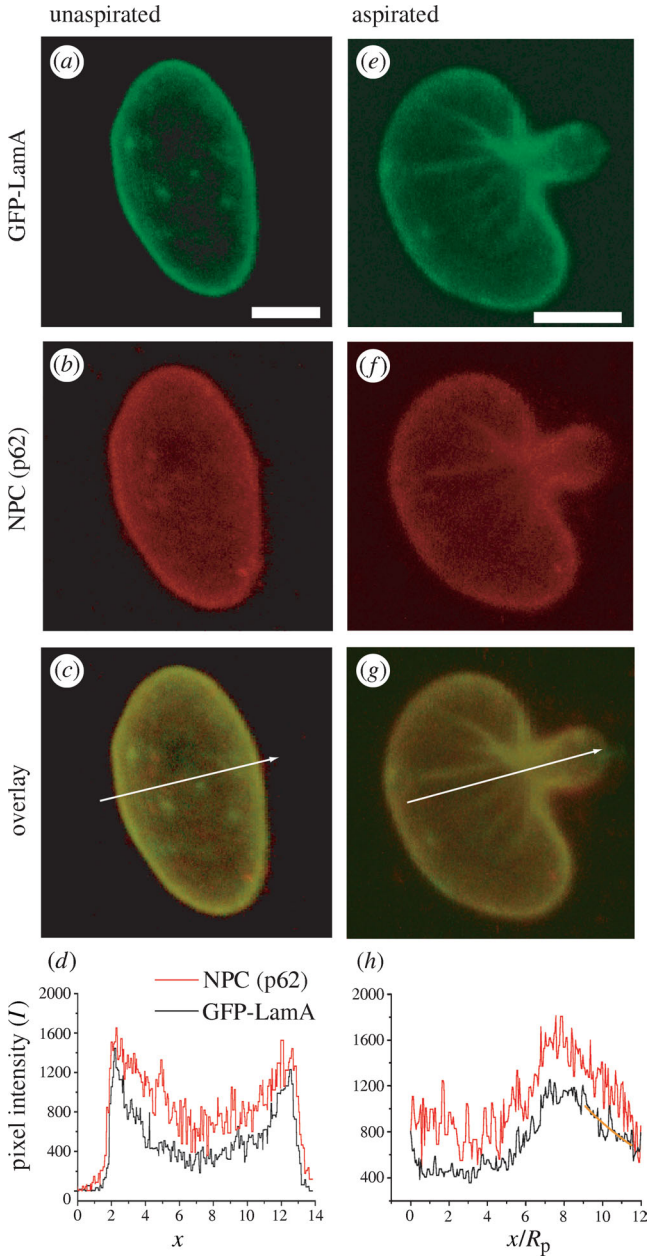

Figure 2. Intensity distribution is the same in *in vitro* nuclei upon aspiration. A nucleus isolated from a *HeLa* cell expressing GFP-LamA (*a*) is deformed by aspiration (*e*). NPCs are visualized by indirect immunofluorescene against nucleoporin p62 (*b*,*f*). Both GFP-LamA and p62 exhibit similar localization at the NE (*c*,*d*) and decays in intensity (*g*,*h*). Buckling of the surface of isolated nuclei upon aspiration (*e*–*g*) illustrates that the NE resists shear forces. Intensity profiles of the three-dimensional reconstructions of nuclei obtained by CIMD are generated by the arrows (*c*,*g*). The maximum intensity corresponds to the mouth of the pipette. The exponential form $\rho(x) \propto \exp(-ax/R_p)$ is fit to the data (orange) and yields $a = 0.41 \pm 0.08$ ($n = 8$, $R_p = 1.9$ μm). Scale bars represent 5 μm.

the mechanics of the NE. Nuclei isolated from *HeLa* cells transiently expressing GFP-LamA (figure 2*a*) exhibit the same decay in $\rho(x)$ as *in vivo* nuclei upon aspiration (figure 2*g*,*h*), $a_{\text{vitro}} = 0.41 \pm 0.08$ ($n = 8$). This correlation between *in vivo* and *in vitro* results demonstrates a remarkable robustness of the NE despite the isolation procedure and *in vitro* buffer conditions. It also shows that NE mechanical properties are solely determined by material within the nucleus.

NPCs visualized by indirect immunofluorescence using an antibody directed against nucleoporin p62 exhibit an intensity gradient similar to that of GFP-LamA upon deformation (figure 2*f*–*h*) which also remains stable over time. This observation indicates a mechanical coherence between NPC and the lamina and is in accordance with observations of a stable lamin-NPC network (Daigle *et al.* 2001) and an insoluble lamin-pore complex (Aaronsen & Blobel 1975). The similar tongue intensity gradient of both NPC and GFP-LamA is very strong evidence that these two NE components are associated with an underlying structure that resists shear forces (i.e. is not fluid).

Further evidence of the solid-like nature of the NE structure is demonstrated by the buckling folds observed in both brightfield (not shown) and

fluorescent images of isolated nuclei (figure 2*e–g*). These folds form parallel to the pipette and radiate out from the mouth in the direction of tension. Additional evidence of the NE's shear rigidity is also seen in the crumpling of the nuclear surface at low aspiration pressures (not shown).

3.3. Viscous and elastic

On a short time-scale (of the order of seconds), nuclear deformations are reversible as nuclei aspirated rapidly in and out of the pipette return to their original form. Partial reversibility is observed on a time-scale of approximately 10 s, whereby the aspirated tongue persists upon expiration of the nucleus from the pipette and relaxes on a longer time-scale. In this case, the nucleus does not return to its unaspirated form on the experimental time-scale (15–20 min). Both *in vivo* and *in vitro* nuclei aspirated over minutes retain their deformed state and exhibit slower relaxation. This behaviour is indicative of the viscoelastic properties of nuclei (Guilak *et al.* 2000).

3.4. Insights into lamina lateral organization

Some simple considerations about the underlying mesoscopic structure that gives rise to this behaviour can be made from the pixel intensity distributions. Analysis of the pixel intensity distribution reveals the following. (i) For an unperturbed NE, no pixels have zero intensity ($I_o > 0$), and thus, the variations in the density must take place on a length-scale that is short compared with the characteristic pixel size, l_{pix}. (ii) Under aspiration of the *in vivo* NE, the mean intensity in the tongue tip, $\langle I_i \rangle$, typically remains less than that in the bulk, $\langle I_o \rangle$ (figure 1*l*). Typically $I_i > 0$, indicating an absence of voids or tears above the length-scale of optical resolution and further verifying that the lamina can withstand large deformations. (iii) Despite the varying intensity for unaspirated and aspirated membranes, an approximate Gaussian form holds in all regions of both unaspirated and aspirated nuclei (figure 1*f*,*l*) and the variances are comparable.

We assume three different modes of random lateral distribution of fluorophores that model the GFP-LamA density decrease caused by (a) homogeneous expansion of the lamina (e.g. regular lattice lamina structure); (b) lateral expansion of NPCs; and (c) expansion of GFP-LamA depleted vacancies (heterogeneous lamina structure). (Consult the Electronic Appendix for details.) (i) The first of these models is the *network lateral expansion model*. The lamina has been depicted as a two-dimensional lattice network (figure 3*a*) that upon aspiration will stretch and undergo areal expansion. This model also describes a decrease in lamin density owing to the in-plane extension/stretching of network undulations. Upon homogeneous area expansion of this model network, both $\langle I \rangle$ and $\sigma(I)$ are reduced. (ii) The second model is the *variable pore size model*. This model considers the NPC as a relatively weakly associated complex of proteins and region devoid of GFP-LamA. Under lateral tension, the NPC area expands. According to this model, the observed change in $\langle I \rangle$ must require large pore dilations beyond the optical resolution and a significant reduction in σ with the intensity. (iii) Third is the *lamin vacancy model*. This model assumes that both the areas containing GFP-LamA and NPCs are constant, but that voids or vacancies appear in the structure upon dilation. Expansion of this structure gives rise to a decrease in $\langle I \rangle$ and modest changes in $\sigma(I)$. Only the behaviour of the third model is in accordance with the observed pixel intensity distributions. Thus in conjunction with the intensity histograms, modelling of the lateral organization of lamin-A indicates a non-homogeneous lateral organization of the NE on mesoscopic length-scales and heterogeneous depletion of GFP-LamA on a length-scale below optical resolution (approximately 250 nm; figure 3).

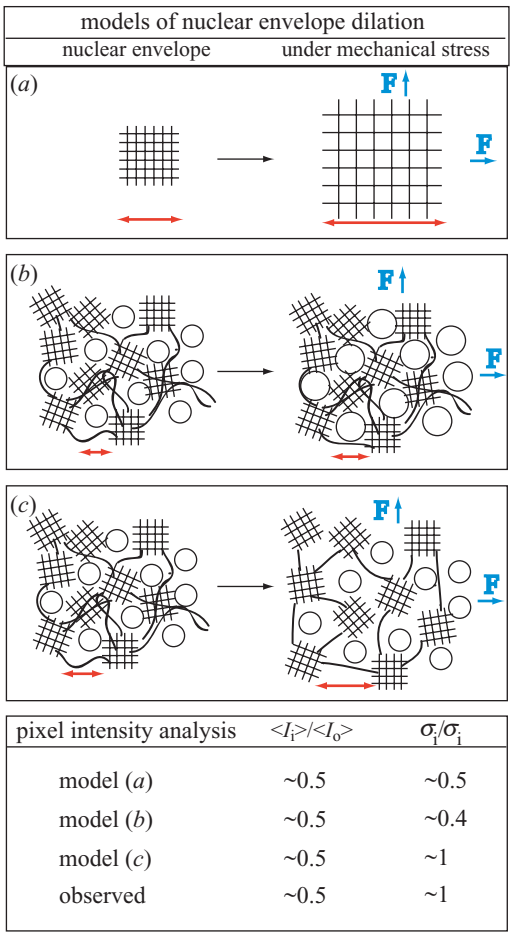

pixel intensity analysis	$\langle I_i \rangle / \langle I_o \rangle$	σ_i / σ_i
model (*a*)	~0.5	~0.5
model (*b*)	~0.5	~0.4
model (*c*)	~0.5	~1
observed	~0.5	~1

Figure 3. Schematics of models for the dilation of the nuclear envelope (NE). A lateral tension, *F*, (such as that induced by micropipette aspiration) results in NE dilation and results in expansion of NE components by a factor, λ. (*a*) Lateral structure of the NE is dominated by a protein network (e.g. regular lattice network of lamins) whose density decreases upon stretching. NPCs are randomly distributed and are not deformed under mechanical stress. (*b*) NPCs (circles) are assumed to be highly flexible and easily undergo dilation while the form of the surrounding lamina meshwork does not yield to mechanical stress. (*c*) The lamina is a heterogeneous meshwork consisting of both regular lattice domains and interconnecting filaments. Under mechanical stress the meshwork expands and vacancies of lamin-A result. NPCs remain constant in form.

4. CONCLUSIONS

Understanding the behaviour of the NE under mechanical stress requires insights into the NE and lamina structure. Given that lamins are coiled-coil proteins (McKeon *et al.* 1986) and the coiled-coil is an elastic structure (Schwaiger *et al.* 2002), a minimal model of a connected lamin network bound to the NE would give rise to elastic behaviour with an intensity decay parameter of $0 < a \leq 2$ upon deformation, consistent with our findings ($a = 0.41$). We demonstrate, however, that NE components in both unaspirated and aspirated nuclei are heterogeneously distributed on mesoscopic length-scales, implying that the lamina is not simply a regular lateral lattice network (figure 3). This finding is consistent with observations of the lateral heterogeneous organization of NE-associated structures (Paddy *et al.* 1990; Makatsori 2004).

Further clues are needed to better understand meso- and microscopic NE structure, but it is clear that the NE encapsulates transcriptional machinery in an elastic yet mechanically resilient compartment that resists shear forces. Considering that shear forces can induce degradation of DNA (Lengsfeld & Anchordoquy 2002), the solid-like nature of the NE may thus serve to protect genetic material. Furthermore, structural changes in the lamina that occur with mitosis, apoptosis, NE-related diseases and viral infection all result in massive alterations in both NE material properties and function. Our method of quantitatively characterizing NE material properties now provides a way to analyse these changes and represents a step towards a deeper understanding of the link between lamina structure and function. Helping to maintain nuclear shape, regulate nuclear composition and facilitate higher levels of cellular organization, the NE is a truly unique material in the architecture of an organelle that plays a core role in the matter of life.

Our thanks to D. K. Shumaker and R. D. Goldman for the gift of GFP-lamin A, J. S. Anderson, Y. W. Lam, and S. E. Ong for helpful discussions, and J.R. Henriksen for initiating the implementation of CIMD. A.C.R. is a Julie Payette Scholar supported by the Natural Scientific and Research Council of Canada. MEMPHYS and CEBI are funded by the Danish National Research Foundation.

REFERENCES

Aaronsen, R. & Blobel, G. 1975 Isolation of nuclear pore complexes in association with a lamina. *Proc. Natl Acad. Sci. USA* **72**, 1007–1011.

Aebi, U., Cohn, J., Buhle, L. & Gerace, L. 1986 The nuclear lamina is a meshwork of intermediate-type filaments. *Nature* **323**, 560–564.

Alberts, B., Johnson, A., Lewis, J., Raff, M., Roberts, K. & Walter, P. 2002 *Molecular biology of the cell.* New York, USA: Garland Science.

Bettinger, B. T., Gilbert, D. M. & Amberg, D. C. 2004 Actin up in the nucleus. *Nature* **5**, 410–415.

Boal, D. 2002 *Mechanics of the cell.* Cambridge, UK: Cambridge University Press.

Daigle, N., Beaudouin, J., Hartnell, L., Imreh, G., Hallberg, E., Lippincott-Schwartz, J. & Ellenberg, J. 2001 Nuclear pore complexes from immobile networks and have a very low turnover in live mammalian cells. *J. Cell Biol.* **154**, 71–84.

Discher, D. E., Mohandas, N. & Evans, E. A. 1994 Molecular maps of red cell deformation: hidden elasticity and *in situ* connectivity. *Science* **266**, 1032–1035.

Evans, E. A. & Needham, D. 1987 Physical properties of surfactant bilayer membranes: thermal transitions, elasticity, rigidity, cohesion, and colloidal interactions. *J. Phys. Chem.* **91**, 4219–4228.

Fawcett, D. W. 1966 On the occurrence of a fibrous lamina on the inner aspect of the nuclear envelope in certain cells of vertebrates. *Am. J. Anat.* **119**, 129–146.

Goldman, R. D., Gruenbaum, Y., Moir, R. D., Shumaker, D. K. & Spann, T. P. 2002 Nuclear lamins: building blocks of nuclear architecture. *Gen. Dev.* **16**, 533–547.

Guilak, F., Tedrow, J. R. & Burrgkart, R. 2000 Viscoelastic properties of the cell nucleus. *Biochem. Biophys. Res. Commun.* **269**, 781–786.

Jackson, D. A., Yuan, J. & Cook, P. R. 1988 A gentle method of preparing cyto- and nucleo-skeletons and associated chromatin. *J. Cell Sci.* **90**, 365–378.

Lammerding, J., Schulze, P. C., Takahashi, T., Kozlov, S., Sullivan, T., Kamm, R. D., Stewart, C. L. & Lee, R. T. 2004 Lamin A/C deficiency causes defective nuclear mechanics and mechanotransduction. *J. Clin. Invest.* **113**, 370–378.

Lengsfeld, C. S. & Anchordoquy, T. J. 2002 Shear-induced degradationofplasmidDNA. *J. Pharm. Sci.* **91**,1581–1589.

Lodish, H., Berk, A., Zipursky, S. L., Matsudaira, P. & Baltimore, D. 2001 *Molecular cell biology.* New York, USA: Freeman and Company.

Makatsori, D. *et al.* 2004 The inner nuclear membrane protein LBR forms distinct microdomains and links epigenetically marked chromatin to the nuclear envelope. *J. Biol. Chem.* **279**, 25567–25573.

Markin, V. S. & Kozlov, M. M. 1988 Mechanical properties of the red cell membrane skeleton: analysis of axisymmetric deformations. *J. Theor. Biol.* **133**, 147–167.

Mattout-Drubezki, A. & Gruenbaum, Y. 2003 Dynamic interactions of nuclear lamina proteins with chromatin and transcriptional machinery. *Cell. Mol. Life Sci.* **60**, 2053–2063.

McKeon, F. D., Kirschner, M. W. & Caput, D. 1986 Homologies in both primary and secondary structure between nuclear envelope and intermediate filament proteins. *Nature* **319**, 463–468.

Moir, R. D., Yoon, M., Khuon, S. & Goldman, R. D. 2000 Nuclear lamins A and B1: different pathways of assembly during nuclear envelope formation in living cells. *J. Cell Biol.* **151**, 1155–1168.

Mounkes, L., Kozlov, S., Burke, B. & Stewart, C. L. 2003 The laminopathies: nuclear structure meets disease. *Curr. Opin. Gen. Dev.* **13**, 223–230.

Muramatsu, M., Smetana, K. & Busch, H. 1963 Quantitative aspects of isolation of nucleoli of the Walker carcinosarcoma and liver of the rat. *Cancer Res.* **25**, 693–697.

Ogden, R. W. 1984 *Non-linear elastic deformations.* Chichester, UK: Ellis Harwood Ltd.

Paddy, M. R., Belmont, A. S., Saumweber, H., Agard, D. A. & Sedat, J. W. 1990 Interphase nuclear envelope lamins form a discontinous network that interacts with only a fraction of the chromatin in the nuclear periphery. *Cell* **62**, 89–106.

Schwaiger, I., Sattler, C., Hostetter, D. R. & Rief, M. 2002 The myosin coiled-coil is a truly elastic protein structure. *Nature* **1**, 232–235.

Shumaker, D. K., Kuczmarski, E. R. & Goldman, R. D. 2003 The nucleoskeleton: lamins and actin are major players

in essential nuclear functions. *Curr. Opin. Cell Biol.* **16**, 358–366.

Stokke, B. T., Mikkelsen, A. & Elgsaeter, A. 1986 The human erythrocyte membrane skeleton may be an ionic gel. III. Micropipette aspiration of unswollen erythrocytes. *J. Theor. Biol.* **123**, 205–211.

Zastrow, M. S., Vlcek, S. & Wilson, K. L. 2004 Proteins that bind A-type lamins: integrating isolated clues. *J. Cell Sci.* **117**, 979–987.

The supplementary Electronic Appendix is available at http://dx.doi.org/10.1098/rsif.2004.0022 or via http://www.pubs.royalsoc.ac.uk.

ELECTRONIC APPENDIX

This is the Electronic Appendix to the article

Characterization of the elastic properties of the nuclear envelope

by

A. C. Rowat, L. J. Foster, M. M. Nielsen, M. Weiss and J. H. Ipsen

J. R. Soc. Interface (doi:10.1098/rsif.2004.0022)

1 Electronic appendix: Modelling of intensity distributions

The characterization of the GFP-LamA pixel intensity (density) distribution on a mesoscopic scale was carried out by assuming random lateral distributions of GFP-LamA. We assume that the lamin density variations are characterized by a single length scale, ξ. The area of the pixel can then be partitioned into $(l_{pix}/\xi)^2$ square cells each with area ξ^2. The total intensity for a pixel is the contributions from the squares which are are not devoid of GFP-LamA: $I = \rho(l_{pix}^2 - \xi^2 n)$ where n is the number of cells devoid of GFP-LamA and ρ is proportional to the density of GFP-LamA in the squares with flourescence contribution[1]. Within the simplified description the configurations of the regions are completely random and the probability distribution for n can be described by a simple binomial distribution:

$$p(n) = \left(\begin{pmatrix} \left(\frac{l_{pix}}{\xi}\right)^2 \\ n \end{pmatrix} \right) \phi^n \, (1-\phi)^{\left(\frac{l_{pix}}{\xi}\right)^2 - n} \tag{1}$$

where ϕ is the area fraction of GFP-LamA devoid regions. The mean and variance in the intensity are $\langle I \rangle = \rho l_{pix}^2 (1-\phi)$ and $\sigma(I) = \rho l_{pix}^2 \left(\frac{l_{pix}}{\xi}\right) \sqrt{\phi(1-\phi)}$. On this basis, we predict the density distributions of three models for the lateral organization of the lamina under lateral expansion.

1.1 Network lateral expansion model

For expansion of a regular lamina network by a factor $\lambda \sim \sqrt{A^i_{LamA}/A^o_{LamA}}$ where A^o_{LamA} is the initial GFP-LamA area, the density of GFP-LamA is reduced by a factor $A^o_{\mathrm{LamA}}/A^i_{\mathrm{LamA}}$. It follows that with area dilation, $\langle I \rangle$ is reduced by $\sim \frac{A^o_{\mathrm{LamA}}}{A^i_{\mathrm{LamA}}}$ while $\sigma(I)$ is reduced by $\sim (\frac{A^o_{\mathrm{LamA}}}{A^i_{\mathrm{LamA}}})^{1.5}$.

[1]Note that GFP-LamA is much smaller ($\sim$ 50nm) than both the optical resolution ($\sim$ 250nm) and l_{pix}, so the intensity of a pixel is the added contribution of fluorophores within a pixel.

1.2 Variable pore size model

Here the important length scale is the NPC diameter, ξ_p. For the unperturbed NE, A_p^o is the area initially occupied by NPCs and $\xi_p^o \sim 40 - 120$ nm varies under lateral stretching of NE. Here, NPCs are considered as regions devoid of GFP-LamA and the area of the surrounding lamina, A_{LamA}, is a constant. The area fraction occupied by NPCs changes during expansion and it follows that an expansion of NPC area gives rise to a small decrease in $\langle I \rangle$ while the relative width of the distribution remains constant: $\frac{\sigma(I)}{\langle I \rangle} = \frac{l_{pix}}{\xi_p^o}\sqrt{\frac{A_p^o}{A_{LamA}}}$.

1.3 Lamin vacancy model

For simplicity we assume that the characteristic length scale, ξ, for the vacancies or voids that appear upon expansion is the same as for the NPCs. The area of such vacancies/voids is denoted by A_{vac}. In this case $\langle I \rangle$ decreases like $\frac{A_{LamA}}{A_{LamA}+A_p^o+A_{vac}}$, and $\frac{\sigma(I)}{\langle I \rangle} = \frac{l_{pix}}{\xi_p^o}\sqrt{\frac{A_p^o+A_{vac}}{A_{LamA}}}$. Thus while the intensity monotonously declines, $\sigma(I)$ changes only modestly over a wide range of $\frac{A_p^o+A_{vac}}{A_{LamA}}$.